INTERNATIONAL JOURNAL FOR NUMERICAL METHODS IN FLUIDS, VOL. 15, 773–789 (1992)

A FINITE DIFFERENCE TECHNIQUE FOR SOLVING THE NEWTONIAN JET SWELL PROBLEM

CHIN-TSU HAN, CHIN-CHIN TSAI, TSAI-AN YU AND TA-JO LIU*

Department of Chemical Engineering, National Tsing Hua University, Hsinchu, Taiwan 300, Republic of China

SUMMARY

A finite difference technique that incorporates a numerical mapping has been successfully applied to analyse both planar and axisymmetric Newtonian jets. A pressure gradient equation and a free-surface slope equation have been derived for free-surface iteration. The computation of pressure inside the jet surface using the pressure gradient equation is stable and accurate at high Reynolds numbers. The free-surface slope equation is needed for updating the free surface and is applicable for jets with strong surface tension effects. The present development can simulate the Newtonian jets for Reynolds numbers as high as 2000 and capillary number as low as 10^{-5}. Numerical predictions by the present technique are close to the results of previous finite element simulations.

KEY WORDS Finite difference method. Newtonian jet swell

INTRODUCTION

Free-surface flows appear in many industrial operations. The simulation of free-surface flows presents a challenging problem because the location of the free surface is unknown and has to be determined simultaneously with the flow field. Three boundary conditions, i.e. the kinematic condition, the tangential stress balance and the normal stress balance, have to be satisfied on the free surface and usually one of the conditions is used to determine the position of the free surface. The jet swell problem has been a popular test case for free-surface flow simulations because experimental and theoretical works are available for comparison. Numerical developments for the jet swell problem were recently reviewed by Tanner.[1] The finite element method (FEM) has been successful for solving the Newtonian jet swell problem. Nickell *et al.*[2] first simulated creeping Newtonian jets, and the kinematic condition was applied for free-surface iteration. Reddy and Tanner[3] and Omodei[4,5] later solved jet swell with significant inertial and surface tension effects. Silliman and Scriven[6] found that if the capillary number Ca is smaller than one, the normal stress balance should be used for free-surface iteration, but if $Ca > 1$, the kinematic condition should be used instead.

Ruschak[7] introduced a boundary location method so that the jet free surface was determined together with the flow field through a full Newton iteration. Kistler and Scriven[8] elaborated this approach and successfully solved the coating flow problem. Georgiou *et al.*[9] also used the same full Newton iteration scheme and obtained the jet swell ratio for Reynolds number Re as high as 2000 and Ca as low as 10^{-5}. Kruyt *et al.*[10] proposed a total linearization method so that

* To whom correspondence should be addressed.

0271–2091/92/190773–17$13.50

Received October 1991
Revised March 1992

free-surface iteration could be implemented easier than the full Newton iteration. Georgiou *et al.*[11] applied the singular finite element method and accelerated the convergence on free-surface iteration with mesh refinement.

Comparing with the FEM, the finite difference method (FDM) appears to have certain merits, such as: the formulation and mesh refinement are easy, and simulation for steady-state problems can be extended to time-dependent problems in a straightforward manner.[12,13] However, the development of the FDM for solving free-surface flow problems has been less popular than the FEM.

Several authors attempted to solve the jet swell problem with a conventional finite difference method. Horsfall[14] analysed the creeping Newtonian jets. Hill *et al.*[15] applied the marker-and-cell method to study the Newtonian jet for $Re>0$. Values of the jet swell ratio computed by these authors are quite different from the predictions based on the finite element method. The errors may come from fitting the jet free surface with grid points.[1]

Recently, several authors avoided a direct fitting of the free surface by grid points through a numerical mapping technique, and the flow regime was transformed into a regular domain for numerical integration. Dutta and Ryan[12] examined the creeping Newtonian jet problem; the kinematic condition was used to update the free surface, and the jet swell ratios they obtained were closer to the finite element predictions than those of previous finite difference studies. Ryskin and Leal[16] solved the bubble deformation problem, and the normal stress balance was applied for updating the free surface. Dandy and Leal[17] applied a full Newton iteration method to determine the free surface together with the flow field simultaneously. Liu *et al.*[13] extended the work of Dutta and Ryan[12] to study the planar Newtonian jet with inertial forces included. They applied a numerical mapping technique, the boundary-fitted co-ordinate transformation method (BFCTM) developed by Thompson *et al.*[18,19] for co-ordinate transformation and they could obtain solutions for Re as high as 100 and Ca as low as 0·1. Later Yu and Liu[20] modified the free-surface iteration scheme of Liu *et al.* and could obtain numerical solutions as accurate as the finite element simulations; however, the maximum Reynolds number in their study was still limited to 100. Yu and Liu[20] found that as Re became large, computing pressure from the Navier–Stokes equation would cause serious oscillations on the jet free surface.

In this paper, we shall describe a new finite difference technique to study the planar and axisymmetric Newtonian jet swell problems. We have derived a pressure gradient equation so that the computation of pressure remains stable and accurate at high Reynolds numbers. A free-surface slope equation that combines the kinematic condition and the normal stress balance has also been derived for updating the free surface. With these developments, we are able to obtain solutions for Re as high as 2000, and Ca as low as 10^{-5}. The numerical solutions we obtained are very close to those based on the finite element method, the maximum difference for the jet swell ratio is less than 0·7%.

MATHEMATICAL FORMULATION

We consider the steady motion of an isothermal, incompressible Newtonian jet emanating from a slit or a circular die as shown in Figure 1(a). We are interested in finding the effects of inertial and surface tension forces on the jet; the gravitational effects are neglected in the present study.

We define a geometrical indicator c to represent two different co-ordinate systems; $c=0$ corresponds to the Cartesian co-ordinate system for the slit die, whereas $c=1$ corresponds to the cylindrical co-ordinate system for the circular die.

The following dimensionless variables are defined in the present analysis:

$$z=\bar{z}/a, \qquad r=\bar{r}/a, \qquad H=h/a,$$
$$u=\bar{u}/\langle v\rangle, \qquad v=\bar{v}/\langle v\rangle, \qquad p=(\bar{p}-p_{\text{atm}})a/\mu\langle v\rangle, \tag{1}$$
$$\varphi=\bar{\varphi}/\langle v\rangle a, \qquad \omega=\bar{\omega}a/\langle v\rangle,$$

where a is the characteristic length; it can be one-half of the slit gap, or the radius of the circular die. $\langle v\rangle$ is defined as the average speed far upstream inside the die, i.e.

$$\langle v\rangle \equiv \frac{1}{(1+c)(3+c)\mu}(-\partial\bar{p}/\partial\bar{z})a^2. \tag{2}$$

The stream function φ and vorticity ω are used as the dependent variables and they are related to the velocity components u and v as follows:

$$u=-\frac{\partial\varphi}{\partial z}\Big/r^c, \qquad v=\frac{\partial\varphi}{\partial r}\Big/r^c, \qquad \omega=\frac{\partial u}{\partial z}-\frac{\partial v}{\partial r}. \tag{3}$$

The equation of continuity is automatically satisfied with the definition of φ. φ and ω are related by

$$\frac{\partial^2\varphi}{\partial z^2}+\frac{\partial^2\varphi}{\partial r^2}-\frac{c}{r}\frac{\partial\varphi}{\partial r}=-r^c\omega \tag{4}$$

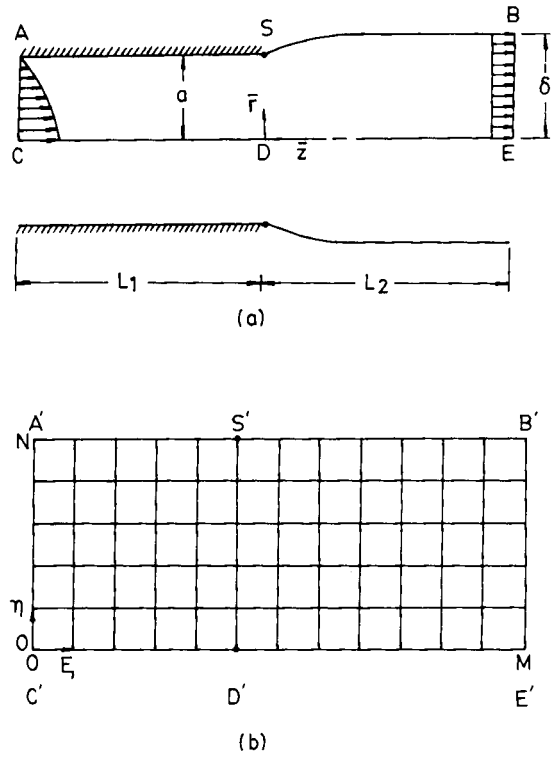

Figure 1. Flow geometry in (a) the physical plane and (b) the transformed plane

and the vorticity transport equation can be obtained after eliminating the pressure terms from the Navier–Stokes equation:

$$\frac{\partial^2\omega}{\partial z^2}+\frac{\partial^2\omega}{\partial r^2}-\frac{c}{r}\frac{\partial\omega}{\partial r}-c\frac{\omega}{r^2}=Re\left(\frac{\partial\varphi}{\partial r}\frac{\partial\omega}{\partial z}-\frac{\partial\varphi}{\partial z}\frac{\partial\omega}{\partial r}+\frac{c}{r}\frac{\partial\varphi}{\partial r}\omega\right)\Big/r^c, \tag{5}$$

where the Reynolds number Re is defined as $Re\equiv\rho\langle v\rangle a/\mu$. The pressure in the whole flow field can be determined from the Navier–Stokes equation.

Equations (4) and (5) are the governing flow equations for the jet problem. Owing to symmetry, we consider only the upper-half of the flow regime as shown in Figure 1(a). If the dimensionless upstream length L_1 and downstream length L_2 are long enough, we can assume that the fluid has the fully developed velocity profiles at AC and BE. The corresponding boundary conditions for φ and ω are as follows:

(B1) at AC (upstream)

$$\varphi=\frac{1}{2}\left(\frac{3+c}{1+c}r^{1+c}-r^{3+c}\right),\qquad \omega=(3+c)r, \tag{6a}$$

(B2) at BE (downstream)

$$\partial\varphi/\partial\xi=0,\qquad \partial\omega/\partial\xi=0, \tag{6b}$$

(B3) on the symmetry line CE

$$\varphi=0,\qquad \omega=0, \tag{6c}$$

(B4) on the wall AS

$$\varphi=1/(1+c),\qquad \omega=-\frac{\partial^2\varphi}{\partial r^2}\Big/r^c, \tag{6d}$$

(B5) on the free surface SB

$$\varphi=1/(1+c) \tag{6e}$$

and ω is evaluated using the tangential stress balance condition (TSBC) that will be derived later.

Three additional boundary conditions have to be satisfied on the free surface. An orthogonal co-ordinate system (s, n, ϕ) is introduced so that the three conditions can be conveniently expressed in this system. Define s as the distance along the free surface, n is the distance along an orthogonal trajectory to the surface and ϕ which is measured from the n-axis is the azimuthal angle. e_s and e_n are unit vectors in the s- and n-direction, respectively. V_s and V_n are the tangential and normal velocity components along the free surface. Define $\theta\equiv\tan^{-1}(u/v)$; then θ is the angle between e_s and the z-axis. Now the three conditions on the free surface are as follows:

(i) the kinematic condition

$$V_n=0, \tag{7a}$$

(ii) the tangential stress balance condition (TSBC)

$$\tau_{sn}=0, \tag{7b}$$

(iii) the normal stress balance condition (NSBC)

$$\tau_{nn}=p+R/Ca, \tag{7c}$$

where the capillary number Ca is defined as $Ca\equiv\mu\langle v\rangle/\sigma$, R is the total curvature defined as $R\equiv-\nabla\cdot e_n$ and the operator (∇) is defined in Appendix II.

We adopt the connection coefficients Γ_{ijk} and scale factors h_s and h_n of Ryskin and Leal[21] to express the stress tensor τ_{sn} and τ_{nn} on the free surface. The derivation of τ_{sn} and τ_{nn} is given in Appendix II, and the results are as follows:

$$\tau_{sn} = \frac{1}{h_n}\frac{\partial V_s}{\partial n} + \Gamma_{nss} V_s, \tag{8a}$$

$$\tau_{nn} = 2\left(\frac{1}{h_n}\frac{\partial V_n}{\partial n} + \Gamma_{nsn} V_s\right). \tag{8b}$$

The velocity components V_s and V_n and ω are as follows:

$$V_s = \frac{1}{h_n}\frac{\partial \varphi}{\partial n}\Big/ r^c, \tag{9a}$$

$$V_n = -\frac{1}{h_s}\frac{\partial \varphi}{\partial s}\Big/ r^c, \tag{9b}$$

$$\omega = -\frac{1}{h_n}\frac{\partial V_s}{\partial n} + \Gamma_{nss} V_s. \tag{9c}$$

Substituting (8a) and (9c) into (7b), we obtain the equation that is used to determine ω on the free surface SB:

$$\omega - 2\Gamma_{nss} V_s = 0. \tag{10}$$

The pressure term appears in the NSBC (7c), Yu and Liu[20] integrated the Navier–Stokes equation to determine pressure and found serious oscillations occurred at high Re. Here we derive a pressure gradient equation to compute pressure on the free surface, and oscillations can be avoided. The s-component of the Navier–Stokes equation is as follows:

$$\frac{1}{h_s}\frac{\partial p}{\partial s} + Re\, V_s \frac{1}{h_s}\frac{\partial V_s}{\partial s} = -\frac{1}{h_n}\frac{\partial \omega}{\partial n} + \Gamma_{n\phi\phi}\omega. \tag{11}$$

We have found that the convection term on the left-hand side of (11) causes numerical instability.

To eliminate $\partial V_s/\partial s$ in (11), the equation of continuity and (8b) have to be used; we obtain the final pressure gradient equation after some manipulation:

$$\frac{1}{h_s}\frac{\partial p}{\partial s} - \frac{1}{2} Re\, V_s p = -\frac{1}{h_n}\frac{\partial \omega}{\partial n} + \Gamma_{n\phi\phi}\omega - Re\, V_s \tfrac{1}{2}(\Gamma_{sns} + \Gamma_{\phi n\phi})/Ca + Re\,\Gamma_{\phi s\phi} V_s^2. \tag{12}$$

A pressure boundary condition is imposed on the jet surface far downstream at point B, i.e.,

$$p - c/(C_0 Ca) = 0, \tag{13}$$

where $C_0 \equiv \delta/a$ is the jet swell ratio. Equation (12) can be integrated from the downstream point B to the separation point S, and pressure along the free surface can be determined.

It is important to note that previous authors[13,20] were using (11) to determine pressure along the free surface. Since the jet becomes unidirectional far downstream, the jet surface should be flat and $\partial V_s/\partial s$ should approach zero. However, as Re is high enough, even if the error for estimating $\partial V_s/\partial s$ on each grid point is small enough, the numerical integration starting from the point B will accumulate this error, and the product of the accumulated error and Re is no longer small. Consequently, p cannot be accurately determined and the previous authors failed to obtain solutions for $Re > 100$. Since the term $\partial V_s/\partial s$ is eliminated, integrating (12) to obtain the pressure

distribution can avoid accumulating numerical errors. A numerical example in the later section will illustrate the difference of using (11) or (12) to compute pressure along the free surface.

Liu *et al.*[13] used the kinematic condition to update the jet free surface and failed to obtain solutions for Ca less than 0·1. Silliman and Scriven[6] found that the kinematic condition should be used to update the free surface if $Ca > 1$, whereas the normal stress balance should be used instead if $Ca < 1$. We have combined the kinematic condition and the NSBC and derived a free-surface slope equation to update the free surface as follows:

$$\frac{1}{Cah_s}\frac{\partial F}{\partial s} - 2V_s\frac{1}{h_n}\frac{\partial F}{\partial n} = (\Gamma_{\phi n\phi}/Ca - p)\sec^2\theta. \tag{14}$$

The derivation of (14) is given in Appendix III; here F is defined as speed ratio (u/v), and on the free surface $F = \tan\theta$ is the slope of the free surface. Since the jet is flat far downstream, or $F = 0$ at B, we can integrate (14) to obtain F on the free surface starting from B. Once F is obtained, we can integrate F starting from the separation point S to determine the position of the free surface.

Equation (14) can be viewed as a combination of the kinematic condition and the NSBC. As $Ca \to 0$, the second term on the left-hand side of (14) becomes negligible, and integrating (14) is similar to integrating the NSBC. On the other hand, as $Ca \to \infty$, the first term on the left-hand side drops out, and (14) reduces to the kinematic condition. Therefore, (14) can be used for either low Ca or high Ca, and we are able to obtain solutions over a wide range $10^{-5} \leqslant Ca \leqslant 10^5$.

CO-ORDINATE TRANSFORMATION

To solve the jet problem, we need to transform the flow geometry in Figure 1(a) to a regular domain for numerical integration. The numerical mapping technique BFCTM developed by Thompson *et al.*[18,19] was adopted. The correspondence between the physical plane (z, r) and the transformed plane (ξ, η) is given in Figure 1(b). The grid distribution can be determined by solving the following mapping equations:

$$\alpha\frac{\partial^2 z}{\partial\xi^2} - 2\beta\frac{\partial^2 z}{\partial\xi\,\partial\eta} + \gamma\frac{\partial^2 z}{\partial\eta^2} = -J^2\left(P\frac{\partial z}{\partial\xi} + Q\frac{\partial z}{\partial\eta}\right), \tag{15a}$$

$$\alpha\frac{\partial^2 r}{\partial\xi^2} - 2\beta\frac{\partial^2 r}{\partial\xi\,\partial\eta} + \gamma\frac{\partial^2 r}{\partial\eta^2} = -J^2\left(P\frac{\partial r}{\partial\xi} + Q\frac{\partial r}{\partial\eta}\right), \tag{15b}$$

in which

$$\alpha = \left(\frac{\partial z}{\partial\eta}\right)^2 + \left(\frac{\partial r}{\partial\eta}\right)^2, \qquad \beta = \frac{\partial z}{\partial\xi}\frac{\partial z}{\partial\eta} + \frac{\partial r}{\partial\xi}\frac{\partial r}{\partial\eta},$$
$$\gamma = \left(\frac{\partial z}{\partial\xi}\right)^2 + \left(\frac{\partial r}{\partial\xi}\right)^2, \qquad J = \frac{\partial z}{\partial\xi}\frac{\partial r}{\partial\eta} - \frac{\partial z}{\partial\eta}\frac{\partial r}{\partial\xi}, \tag{15c}$$

where J is the Jacobian of the transformation. P and Q are forcing functions that can be assigned arbitrarily to regulate mesh distribution.

Dirichlet boundary conditions are imposed on the boundary of the regular domain in the transformed plane and the procedure for solving (15) is identical to that of Reference 13.

The flow equations (4) and (5) are also transformed to the (ξ, η) plane:

$$\alpha\frac{\partial^2\varphi}{\partial\xi^2} - 2\beta\frac{\partial^2\varphi}{\partial\xi\,\partial\eta} + \gamma\frac{\partial^2\varphi}{\partial\eta^2} + J^2\left[\left(P + \frac{c}{rJ}\frac{\partial z}{\partial\eta}\right)\frac{\partial\varphi}{\partial\xi} + \left(Q - \frac{c}{rJ}\frac{\partial z}{\partial\xi}\right)\frac{\partial\varphi}{\partial\eta}\right] = -\omega r^c J^2, \tag{16}$$

and

$$\alpha\frac{\partial^2\omega}{\partial\xi^2}-2\beta\frac{\partial^2\omega}{\partial\xi\,\partial\eta}+\gamma\frac{\partial^2\omega}{\partial\eta^2}+R_1\frac{\partial\omega}{\partial\xi}+R_2\frac{\partial\varphi}{\partial\eta}+R_3\omega=0. \tag{17}$$

The coefficients R_1, R_2 and R_3 are as follows:

$$R_1=-\frac{cJ}{r}\frac{\partial z}{\partial\eta}-\frac{ReJ}{r^c}\frac{\partial\varphi}{\partial\eta}+J^2P, \tag{18a}$$

$$R_2=\frac{cJ}{r}\frac{\partial z}{\partial\xi}+\frac{ReJ}{r^c}\frac{\partial\varphi}{\partial\xi}+J^2Q, \tag{18b}$$

$$R_3=-\frac{cJ^2}{r^2}-\frac{c\,ReJ}{r^{c+1}}\left(\frac{\partial r}{\partial\eta}\frac{\partial\varphi}{\partial\xi}-\frac{\partial r}{\partial\xi}\frac{\partial\varphi}{\partial\eta}\right). \tag{18c}$$

Once φ is determined, the velocity components can be computed as follows:

$$u=-\frac{\partial\varphi}{\partial z}\Big/r^c=-\left(\frac{\partial r}{\partial\eta}\frac{\partial\varphi}{\partial\xi}-\frac{\partial r}{\partial\xi}\frac{\partial\varphi}{\partial\eta}\right)\Big/r^cJ, \tag{19a}$$

$$v=\frac{\partial\varphi}{\partial r}\Big/r^c=-\left(\frac{\partial z}{\partial\eta}\frac{\partial\varphi}{\partial\xi}-\frac{\partial z}{\partial\xi}\frac{\partial\varphi}{\partial\eta}\right)\Big/r^cJ. \tag{19b}$$

Boundary conditions in the transformed plane are:

(T1) on A′C′

$$\varphi=\frac{1}{2}\left(\frac{3+c}{1+c}r^{1+c}-r^{3+c}\right),\qquad \omega=(3+c)r, \tag{20a}$$

(T2) on B′E′

$$\partial\varphi/\partial\xi=0,\qquad \partial\omega/\partial\xi=0, \tag{20b}$$

(T3) on C′E′

$$\varphi=0,\qquad \omega=0, \tag{20c}$$

(T4) on A′S′

$$\varphi=1/(1+c),\qquad \omega=-\gamma\frac{\partial^2\varphi}{\partial\eta^2}\Big/(r^cJ^2), \tag{20d}$$

(T5) on S′B′

$$\varphi=1/(1+c),\qquad \omega=2\Gamma_{nss}\gamma^{0\cdot5}\frac{\partial\varphi}{\partial\eta}\Big/(r^cJ). \tag{20e}$$

The pressure gradient equation and the free-surface slope equation have the following forms in the transformed plane:

$$\frac{\partial p}{\partial\xi}+a_1(\xi,\eta)p=b_1(\xi,\eta), \tag{21}$$

$$\frac{\partial F}{\partial\xi}+a_2(\xi,\eta)\frac{\partial F}{\partial\eta}=b_2(\xi,\eta). \tag{22}$$

The coefficients are:

$$a_1 = -\frac{\gamma Re}{2r^c J}\frac{\partial \varphi}{\partial \eta}, \tag{23a}$$

$$b_1 = \beta\frac{\partial \omega}{\partial \xi}\Big/ J - \gamma\frac{\partial \omega}{\partial \eta}\Big/ J + \Gamma_{n\phi\phi}\omega + a_1(\Gamma_{sns} + \Gamma_{\phi n\phi})/Ca + Re\,\Gamma_{\phi s\phi}\gamma^{1.5}\left(\frac{\partial \varphi}{\partial \eta}\right)^2\Big/(r^{2C}J^2), \tag{23b}$$

$$a_2 = -\frac{2\gamma^{1.5}}{r^c J^2}\frac{\partial \varphi}{\partial \eta}\Big/\left(\frac{1}{Ca} + \frac{2\beta\gamma^{0.5}}{r^c J^2}\frac{\partial \varphi}{\partial \eta}\right), \tag{23c}$$

$$b_2 = \left(\frac{1}{Ca}\Gamma_{\phi n\phi} - p\right)\gamma^{1.5}\Big/\left\{\left(\frac{\partial z}{\partial \xi}\right)^2\left[1/Ca + 2\beta\gamma^{0.5}\frac{\partial \varphi}{\partial \eta}\Big/(J^2 r^c)\right]\right\}. \tag{23d}$$

The connection coefficients in the transformed plane are as follows:

$$\Gamma_{sns} = -\Gamma_{nss} = \left(\frac{\partial^2 z}{\partial \xi^2}\frac{\partial r}{\partial \xi} - \frac{\partial^2 r}{\partial \xi^2}\frac{\partial z}{\partial \xi}\right)\Big/\gamma^{1.5},$$

$$\Gamma_{nsn} = -\Gamma_{snn} = \left[\gamma\left(\frac{\partial^2 r}{\partial \xi \partial \eta}\frac{\partial z}{\partial \xi} - \frac{\partial^2 z}{\partial \xi \partial \eta}\frac{\partial r}{\partial \xi}\right) - \beta\left(\frac{\partial^2 r}{\partial \xi^2}\frac{\partial z}{\partial \xi} - \frac{\partial^2 z}{\partial \xi^2}\frac{\partial r}{\partial \xi}\right)\right]\Big/(J\gamma^{1.5}),$$

$$\Gamma_{\phi s\phi} = -\Gamma_{s\phi\phi} = \frac{c}{r}\frac{\partial r}{\partial \xi}\Big/\gamma^{0.5}, \tag{24}$$

$$\Gamma_{\phi n\phi} = -\Gamma_{n\phi\phi} = \frac{c}{r}\frac{\partial z}{\partial \xi}\Big/\gamma^{0.5},$$

NUMERICAL PROCEDURE

It takes three steps to solve the jet problem numerically; the first two steps, i.e. numerical mapping and solution of the flow equations, are similar to the work of Liu *et al.*[13] and are explained only briefly here. The third step which is used to update the free surface is different from previous studies, and a detailed explanation is necessary.

Numerical mapping

(1) For a given set of (Re, Ca), select the dimensionless upstream length L_1 and downstream length L_2 so that the assumption that fluid flow has the fully developed velocity profiles is not violated. The upstream length L_1 was fixed to be 3 in the present study. As Re goes up, L_2 has to be longer; we followed the suggestion of Georgiou *et al.*[9] to select L_2.
(2) Guess an initial profile for the free surface; we selected $H = 1$ for all the cases.
(3) Set up proper boundary conditions for the mapping equations, more boundary points are imposed in the neighbourhood of the separation point S. Guess an internal grid distribution.
(4) Select proper forcing functions P and Q. Liu *et al.*[13] fixed $P = Q = 0$ in their study, but the grid lines in the r-direction were slightly curved, particularly in the neighbourhood of the separation point. This may be corrected by selecting

$$P = -\frac{\alpha}{J^2}\left(\frac{\partial^2 z}{\partial \xi^2}\right)\Big/\left(\frac{\partial z}{\partial \xi}\right), \qquad Q = 0. \tag{25}$$

Once the grid lines in the r-direction are not curved, more accurate numerical solutions can be obtained.

(5) The mapping equations are discretized with standard central-difference formulas and the discrete system is solved by the successive line overrelaxation method.

Solution of the flow equations

(1) Give guessed values (φ, ω) for all interior grid points.

(2) Apply the successive line underrelaxation method to solve the discrete flow equations. Again, standard second-order difference formulas are used to discretize the flow equations.

Updating the free surface

(1) The pressure gradient equation (21) is discretized in the middle of two grid points i and $i+1$, i.e.

$$\left(\frac{\partial p}{\partial \xi}\right)_{i+1/2} = (p_{i+1} - p_i)/2\Delta\xi, \tag{26a}$$

$$p_{i+1/2} = (p_{i+1} + p_i)/2, \tag{26b}$$

$$(a_1)_{i+1/2} = [(a_1)_{i+1} + (a_1)_i]/2, \tag{26c}$$

$$(b_1)_{i+1/2} = [(b_1)_{i+1} + (b_1)_i]/2. \tag{26d}$$

Substituting (26) into (21), we obtain

$$p_i = \left\{\left[\frac{1}{\Delta\xi} + \frac{1}{2}(a_1)_{i+1/2}\right] p_{i+1} - (b_1)_{i+1/2}\right\} \Big/ \left[\frac{1}{\Delta\xi} - \frac{1}{2}(a_1)_{i+1/2}\right]. \tag{27}$$

The boundary condition (13) for pressure is given on the grid point B′ (M, N); so we can use (27) to determine p from point B′ to point S′. Values of p are needed in the free-surface slope equation.

(2) To solve the free-surface slope equation (22), we first expand the term $\partial F/\partial \eta$ as follows:

$$\left(\frac{\partial F}{\partial \eta}\right)^{k+1}_{i,N} = (3F^{k+1}_{i,N} - 4F^{k}_{i,N-1} + F^{k}_{i,N-2})/2\Delta\eta, \tag{28}$$

where k stands for iteration number, $k+1$ is the current iteration number and k is the previous iteration number. $F^{k+1}_{i,N}$ is the unknown that has to be determined. Substituting (28) into (22), we have

$$\frac{\partial F}{\partial \xi} + \frac{3}{2\Delta\eta} a_2(\xi, \eta) F = b_2(\xi, \eta) + a_2(\xi, \eta)(4F^{k}_{i,N-1} - F^{k}_{i,N-2})/2\Delta\eta. \tag{29}$$

The mathematical form of (29) is similar to (21); therefore, (29) can be discretized in the same way as (26). On B′, $F_{M,N} = 0$; so we can integrate (29) from B′ to S′, i.e. the slope on the free surface is completely determined.

(3) Once F is determined, we can obtain the free-surface position $H(z)$ by integrating F numerically starting from the separation point S:

$$H(z) = \int_0^z F \, dz. \tag{30}$$

(4) Test for convergence. If the maximum difference between the current values of φ, ω and $H(z)$ and the previous values is smaller than a preset tolerance, the computation is complete; otherwise, replace the old values of φ, ω and $H(z)$ by the current values and start the iteration again from Step (4) in Numerical Mapping.

RESULTS AND DISCUSSION

In the present study, all the computations were carried out on a HP 9000/835 machine. The tolerance of convergence for φ, ω and $H(z)$ was fixed to be 1.0×10^{-4}. The relaxation factor for the mapping equations was 1·5 and was between 0·8 and 1·0 for the flow equations. Since a longer L_2 is required as Re increases, the suggestion of Georgiou *et al.*[9] was followed to select an appropriate L_2 for a given Re. The residual of the downstream pressure condition (13) was computed if the residual was less than 10^{-6}; L_2 was considered to be long enough. We found that L_2 suggested by Georgiou *et al.*[9] was adequate for the present finite difference simulation.

We first check the pressure distribution inside the free surface for a planar Newtonian jet. Liu *et al.*[13] failed to obtain solutions for $Re > 100$ and Yu and Liu[20] found that iteration on pressure was very slow to converge if the Navier–Stokes equation was used to determine pressure distribution inside the jet surface and oscillations would appear if Re was too high. We first solved the planar Newtonian jet problem for $Re = 100$ and $Re = 200$, then we used the pressure gradient equation to compute the pressure distribution inside the jet surface. The pressure distribution was also computed using the method of Liu *et al.*[13] i.e. integrating the Navier–Stokes equation. The results are shown in Figure 2. It is easy to see from the NSBC (7c) that as Re becomes large, the viscous term τ_{nn} becomes negligible and the pressure force is balanced by the surface tension force. If the curvature of the jet surface goes to zero, the pressure should approach zero, too. The curvature of the jet surface varies rapidly at the die exit, but it soon approaches zero at a certain distance from the separation point. The pressure distribution should behave similarly. The pressure distribution predicted by the pressure gradient equation is consistent with this behaviour as indicated by the curves in Figure 2, whereas the results based on the method of Liu *et al.*[13]

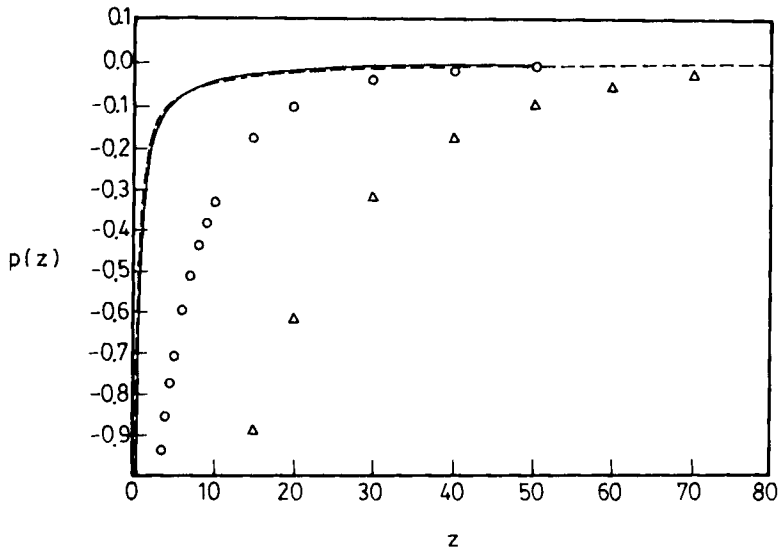

Figure 2. Planar jet: the pressure distribution inside the jet surface with $Ca = 10^5$. $Re = 100$: —— present work; ○ values based on the method of Liu *et al.* (1991); $Re = 200$: – – – present work; △ values based on the method of Liu *et al.* (1991)

appear to be incorrect. This explains that using the pressure gradient equation to compute pressure can extend the range of convergence from $Re = 100$ to $Re = 2000$.

The CPU time for several cases is given in Table I. As Re increases, L_2 is longer and more grid points are needed. Since the initial profile was selected to be $H = 1$ for each case, it required less computing time for the case of high surface tension or small Ca because the free-surface profile was closer to $H = 1$. Comparing the case $Re = 0$ with $Re = 1000$, we observe that although the number of grid points increases 6–8 times, the CPU time required is increased only 5–7 times. This is quite different from the situation if the full Newton iteration as proposed by Dandy and Leal[17] is applied; CPU time would increase significantly as the number of grid points increases.

Table I. CPU time required for nine cases

			Planar jet		Axisymmetric jet	
Re	Ca	L_2	Grid points	CPU time (unit)*	Grid points	CPU time (unit)†
0	10^5	25	21 × 181	1	21 × 181	1
	1			0·701		0·652
	10^{-5}			0·090		0·488
100	10^5	100	21 × 481	1·322	21 × 661	2·482
	1			1·118		2·302
	10^{-5}			0·231		1·950
1000	10^5	500	21 × 1531	5·501	21 × 1201	7·231
	1			4·549		6·977
	10^{-5}			3·128		4·080

* 1 unit = 15·1 min on the HP 9000/835 machine (−O1 compiler).
† 1 unit = 18·0 min on the HP 9000/835 machine (−O1 compiler).

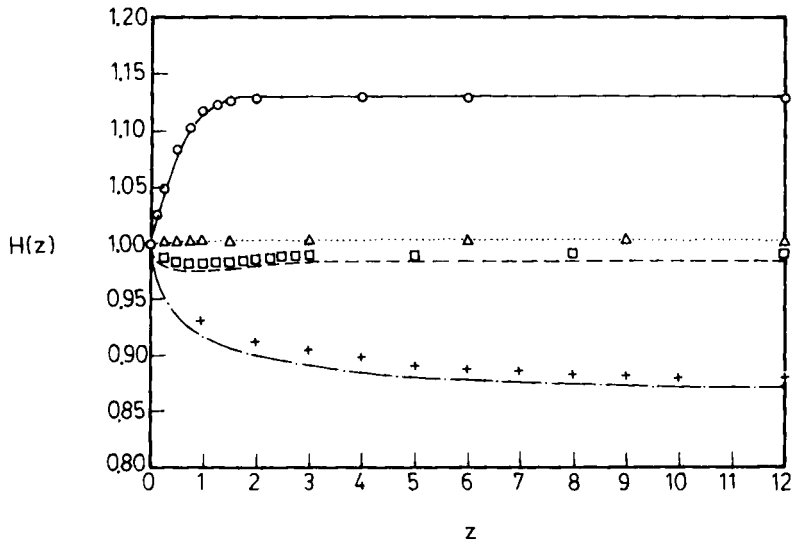

Figure 3. Axisymmetric jet: the effect of Ca on the jet free-surface profiles at low Reynolds numbers. (1) $Re = 0$, $Ca = 10^5$: —— present work; ○ Georgiou *et al.* (1988). (2) $Re = 0$, $Ca = 10^{-2}$: . . . . present work; △ Georgiou *et al.* (1988). (3) $Re = 8$, $Ca = 10^5$: – – – present work; □ Georgiou *et al.* (1988). (4) $Re = 10$, $Ca = 10^5$: –·–·– present work + Georgiou *et al.* (1988)

The free-surface profiles we simulated were compared with the predictions of Georgiou *et al.*[9] for axisymmetric jets in Figures 3 and 4 and with the predictions of Omodei[5] for planar jets in Figure 5. Figure 3 displays the effect of surface tension on the jet surface at low Reynolds numbers; Figures 4 and 5 show the effect of Reynolds number. It is clear that the profiles we computed are close to the finite element simulations over a wide range of *Re* and *Ca*.

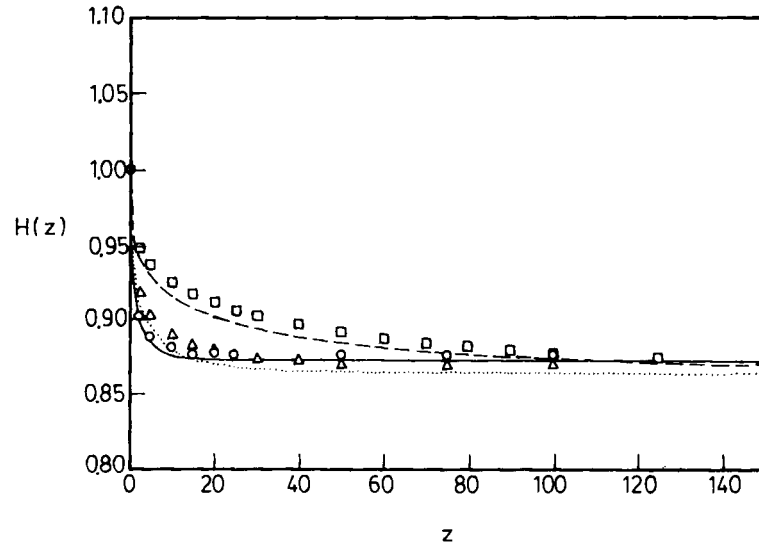

Figure 4. Axisymmetric jet: the effect of *Re* on the jet free-surface profiles with $Ca = 10^5$. (1) $Re = 100$: —— present work; ○ Georgiou *et al.* (1988). (2) $Re = 300$: – – – present work; □ Georgiou *et al.* (1988). (3) $Re = 2000$: . . . . present work; △ Georgiou *et al.* (1988)

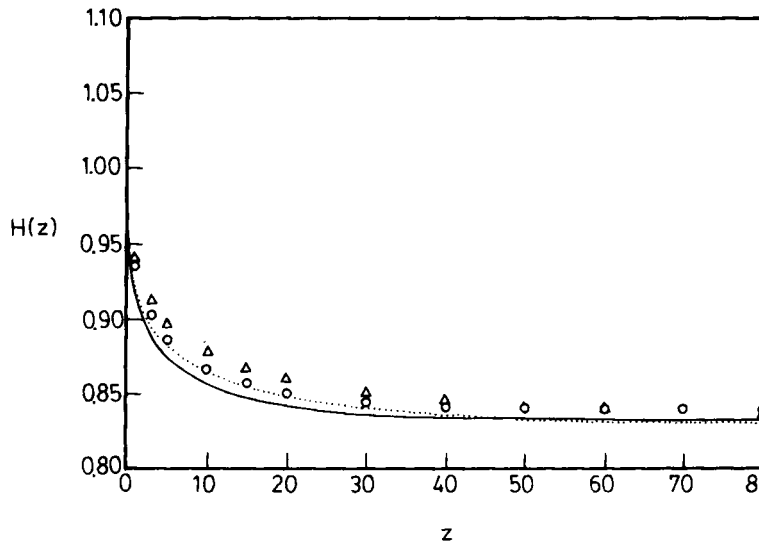

Figure 5. Planar jet: the effect of *Re* on the jet free-surface profiles with $Ca = 10^5$. $Re = 300$: —— present work; ○ Omodei (1979). $Re = 500$: . . . . present work △ Omodei (1979)

The jet swell ratio C_0 as a function of Re is given in Figure 6. Values of C_0 determined by the present development are close to those computed by Georgiou *et al.*[9] The maximum difference is approximately less than 0.7%. The effect of Ca on the jet swell ratio C_0 for an axisymmetric jet is shown in Figure 7. Values of C_0 determined by Georgiou *et al.*[9] are also given in the figure. Similarly, our predictions are in good agreement with those of Georgiou *et al.*[9]

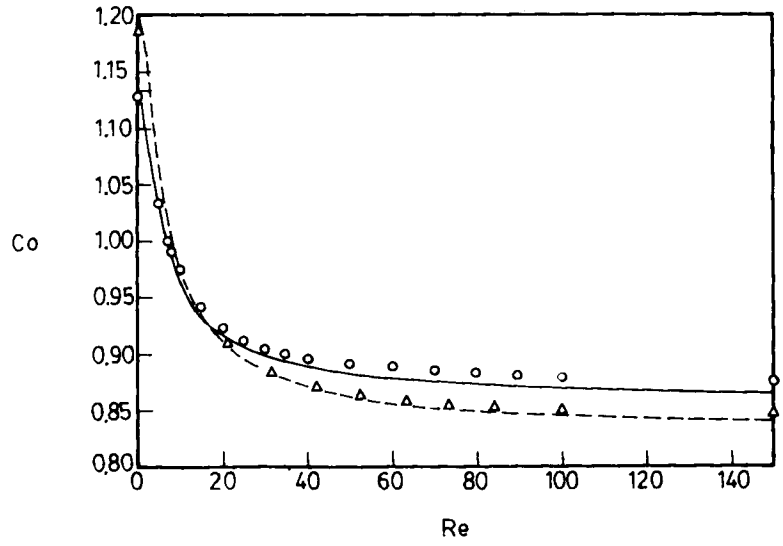

Figure 6. The jet swell ratio C_0 as a function of Re with $Ca = 10^5$. Planar jet: – – – present work; △ Georgiou *et al.* (1988). Axisymmetric jet: —— present work; ○ Georgiou *et al.* (1988)

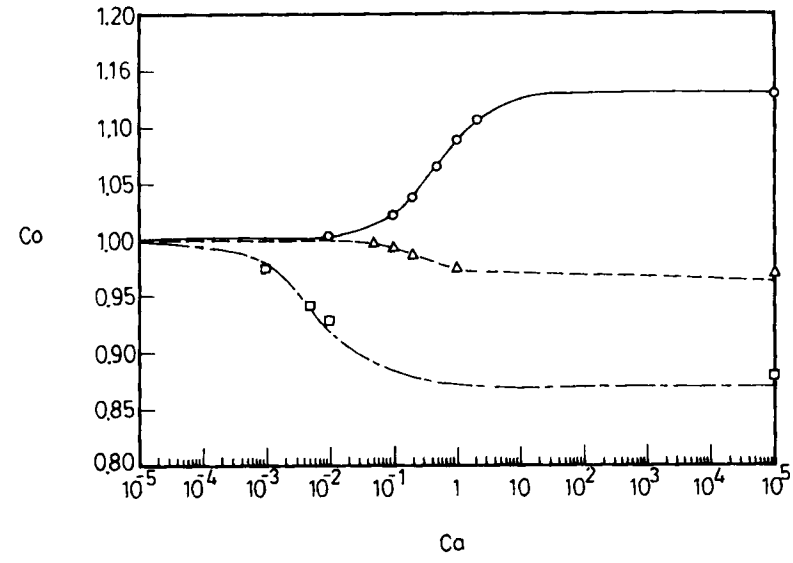

Figure 7. Axisymmetric jet: the effect of Ca on the jet swell ratio C_0. (1) $Re = 0$: —— present work; ○ Georgiou *et al.* (1988). (2) $Re = 10$: —— present work; △ Georgiou *et al.* (1988). (3) $Re = 100$: – – – Present work; □ Georgiou *et al.* (1988)

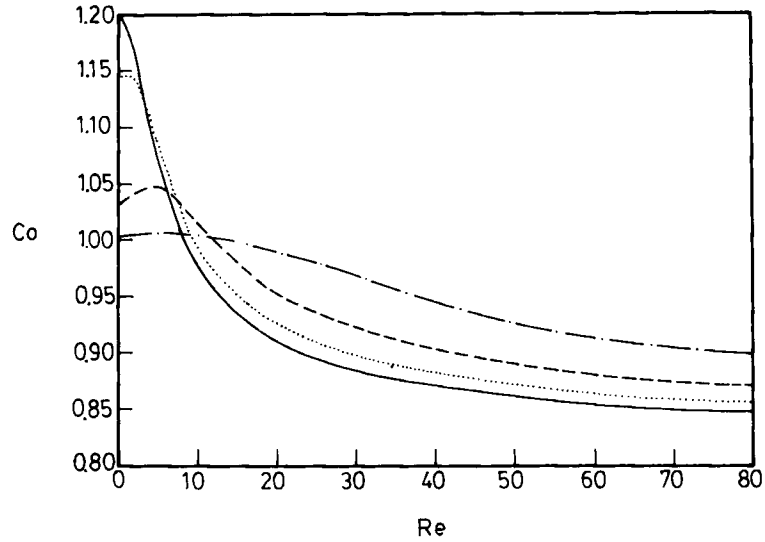

Figure 8. Planar jet: the jet swell ratio C_0 as functions of Re and Ca. (1)——$Ca=10^5$; (2) . . . . $Ca=1$; (3) – – –$Ca=10^{-1}$; (4) —·—$Ca=10^{-2}$

Figure 8 presents the jet swell ratio C_0 as functions of Re and Ca over a wide range for a planar jet. Apparently, the effect of surface tension is important if Ca is less than one. As Re is higher than 15, the jet will shrink instead of swelling. If Ca is small, the jet will swell first and then shrink as Re goes up, and the maximum values of C_0 can be found in the range $5 \leqslant Re \leqslant 10$.

We also checked if the conservation of mass was satisfied on the free surface. The residuals of the conservation of mass were computed and we found the values are much smaller than those of the previous studies.[12,13] The maximum error appears on the separation point and has an order $O(1)$, but the residuals decay rapidly along the jet free surface.

CONCLUSIONS

We have developed a finite difference technique for solving the Newtonian jet swell problem. The finite difference technique incorporates a numerical mapping so that the flow regime is transformed to a regular domain for numerical integration.

We have derived a pressure gradient equation to compute the pressure distribution along the jet surface. Integrating this equation to obtain pressure is a more accurate procedure than a direct integration of the Navier–Stokes equation. A free-surface slope equation has also been derived to update the free surface during the iteration process. This equation can be viewed as a combination of the kinematic condition and the normal stress balance condition. With these two equations, we are able to obtain solutions for Reynolds numbers as high as 2000 and capillary numbers as low as 10^{-5}.

Numerical solutions for both planar and axisymmetric jets have been obtained and the theoretical predictions based on the present development are in good agreement with the results based on the finite element simulations. Values of the jet swell ratio as functions of the Reynolds number and capillary number have been presented.

ACKNOWLEDGEMENT

This research was supported by the National Science Council, the Republic of China, under Grant No. NSC 79-0405-E007-04.

APPENDIX I: NOTATION

a	characteristic length
a_1, b_1	coefficients of the pressure gradient equation, [equation (21)]
a_2, b_2	coefficients of the free-surface slope equation, [equation (22)]
c	geometrical indicator
Ca	capillary number $(=\mu\langle v\rangle/\sigma)$
C_0	jet swell ratio $(=\delta/a)$
e_s, e_n	tangential and normal unit vectors on the free surface
F	speed ratio $(=u/v)$
h, H	location of the free surface, dimensional and dimensionless
h_s, h_n	scale factors, Appendix A
i	index
J	Jacobian of the mapping equations, [equation (15c)]
k	iteration number
M, N	numbers of grid points in the transformed plane
$\bar{p}, p$	fluid pressure, dimensional and dimensionless
P, Q	forcing functions
p_{atm}	atmospheric pressure
R	total curvature $(=-\nabla\cdot e_n)$
R_1, R_2, R_3	coefficients of equation (17)
Re	Reynolds number $(=\rho\langle v\rangle a/\mu)$
s, n, ϕ	orthogonal co-ordinate system on the free surface
$\bar{u}, u$	velocity component in the r-direction, dimensional and dimensionless
$\bar{v}, v$	velocity component in the z-direction, dimensional and dimensionless
V_n, V_s	tangential and normal velocity components on the free surface
$\langle v\rangle$	average fluid speed upstream in the die
$(\bar{z}, \bar{r}), (z, r)$	co-ordinates in the physical plane, dimensional and dimensionless

Greek letters

α, β, γ	coefficients of the mapping equations, as in equation (15c)
δ	one-half of the final jet thickness
$\Delta\xi, \Delta\eta$	mesh sizes in the transformed plane
Γ_{ijk}	connection coefficients
θ	the angle between e_s and the z-axis
μ	fluid viscosity
ξ, η	co-ordinates in the transformed plane
ρ	fluid density
σ	surface tension coefficient
$\bar{\varphi}, \varphi$	stream function, dimensional and dimensionless
$\bar{\omega}, \omega$	vorticity, dimensional and dimensionless

APPENDIX II: VARIABLES IN THE CO-ORDINATE SYSTEM (s, n, ϕ)

The velocity components V_s and V_n are related to u and v as follows:

$$V_s = v\cos\theta + u\sin\theta, \tag{31}$$

$$V_n = -v\sin\theta + u\cos\theta. \tag{32}$$

The operator ∇ is defined as

$$\nabla = \frac{1}{h_s}\frac{\partial}{\partial s}e_s + \frac{1}{h_n}\frac{\partial}{\partial n}e_n + \frac{1}{r^c}\frac{\partial}{\partial \phi}e_\phi, \tag{33}$$

where the scale factors h_s and h_n are defined as

$$h_s^2 = \left(\frac{\partial z}{\partial s}\right)^2 + \left(\frac{\partial r}{\partial s}\right)^2, \tag{34}$$

$$h_n^2 = \left(\frac{\partial z}{\partial n}\right)^2 + \left(\frac{\partial r}{\partial n}\right)^2. \tag{35}$$

The connection coefficients Γ_{ijk} are needed in co-ordinate transformation. A given Γ_{ijk} represents the i-component of the rate of change in e_j along e_k. There are eight non-zero connection coefficients;[16] they are related to the scale factors as follows:

$$\begin{aligned}
\Gamma_{sns} &= -\Gamma_{nss} = \frac{1}{h_s h_n}(\partial h_s/\partial n) \\
\Gamma_{nsn} &= -\Gamma_{snn} = \frac{1}{h_s h_n}(\partial h_n/\partial s), \\
\Gamma_{\phi s\phi} &= -\Gamma_{s\phi\phi} = \frac{c}{r h_s}(\partial r/\partial s), \\
\Gamma_{\phi n\phi} &= -\Gamma_{n\phi\phi} = \frac{c}{r h_n}(\partial r/\partial n).
\end{aligned} \tag{36}$$

The stress tensor τ is defined as $\tau \equiv (\nabla \mathbf{v} + \nabla \mathbf{v}^{\mathrm{T}})$, and the components τ_{sn} and τ_{nn} can be found by substituting the conditions $V_n = 0$ and $\partial V_n/\partial s = 0$ into the definition:

$$\begin{aligned}
\tau_{sn} &= \frac{1}{h_n}\frac{\partial V_s}{\partial n} + \Gamma_{nss} V_s, \\
\tau_{nn} &= 2\left(\frac{1}{h_n}\frac{\partial V_n}{\partial n} + \Gamma_{nsn} V_s\right).
\end{aligned} \tag{37}$$

APPENDIX III: DERIVATION OF THE FREE-SURFACE SLOPE EQUATION (14)

We have on the free surface

$$V_n = 0, \tag{38}$$

$$u = v \tan\theta \tag{39}$$

and from (31), we obtain V_s on the free surface as follows:

$$V_s = v \sec\theta. \tag{40}$$

Differentiating (32) with respect to n and substituting (38)–(40) into the resulting equation we obtain

$$\frac{\partial V_n}{\partial n} = -V_s\frac{\partial \theta}{\partial n} + V_s\frac{\partial \theta}{\partial n} = 0 \tag{41}$$

on the free surface. Therefore (8b) reduces to

$$\tau_{nn} = 2\Gamma_{nsn} V_s. \tag{42}$$

The total curvature R is defined as

$$R \equiv -\nabla \cdot e_n = -(\Gamma_{sns} + \Gamma_{\phi n \phi}). \tag{43}$$

We define F as the ratio of u to v, and on the free surface we have $F \equiv (u/v) = \tan\theta$; therefore, F reduces to the slope of the free surface on the jet surface. From the definition of Γ_{nsn} and Γ_{sns}, we have

$$\Gamma_{nsn} = \frac{1}{h_n}\frac{\partial\theta}{\partial n} = \frac{1}{h_n}\frac{\partial F}{\partial n}\cos^2\theta, \tag{44}$$

$$\Gamma_{sns} = -\frac{1}{h_s}\frac{\partial\theta}{\partial s} = \frac{-1}{h_s}\frac{\partial F}{\partial s}\cos^2\theta. \tag{45}$$

combining (42) and (43), (44) and (45), and then substituting the results into the NSBC (7c), we obtain the free-surface slope equation (14).

REFERENCES

1. R. I. Tanner, *Engineering Rheology*, Clarendon Press, Oxford, 1988.
2. R. E. Nickell, R. I. Tanner and B. Caswell, 'The solution of viscous incompressible jet and free-surface flows using finite-element methods', *J. Fluid Mech.*, **65**, 189–206 (1974).
3. K. R. Reddy and R. I. Tanner, 'Finite-element solution of viscous jet flow with surface tension', *Comput. Fluids*, **6**, 83–91 (1978).
4. B. J. Omodei, 'Computer solutions of a plane Newtonian jet with surface tension', *Comput. Fluids*, **7**, 79–96 (1979).
5. B. J. Omodei, 'On the Die-Swell of an axisymmetric Newtonian jet', *Comput. Fluids*, **8**, 275–289 (1980).
6. W. J. Silliman and L. E. Scriven, 'Separating flow near a static contact line: slip at a wall and shape of a free surface', *J. Comput. Phys.*, **34**, 287–313 (1980).
7. K. J. Ruschak, 'A method for incorporating free boundary with surface tension in finite-element fluid-flow simulators', *Int. j. numer. methods eng.*, **15**, 639–648 (1980).
8. S. F. Kistler and L. E. Scriven, 'Coating flows', in J. R. A. Pearson and S. M. Richardson (eds.), *Computational Analysis of Polymer Processing*, Chap. 8, Applied Science Publishers London, 1983.
9. G. C. Georgiou, T. C. Papanastasiou and J. O. Wilkes, 'Laminar Newtonian jets at high Reynolds number and high surface tension', *AIChE J.*, **34**, 1559–1562 (1988).
10. N. P. Kruyt, C. Cuvelier, A. Segal and J. van Der Zanden, 'A total linearization method for solving viscous free boundary flow problems by the finite element method', *Int. j. numer. methods fluids*, **8**, 351–363 (1988).
11. G. C. Georgiou, W. W. Schultz and L. G. Olson, 'Singular finite elements for the sudden-expansion and the die-swell Problems', *Int. j. numer. methods fluids*, **10**, 357–372 (1990).
12. A. Dutta and M. E. Ryan, 'Dynamics of a creeping Newtonian jet with gravity and surface tension: a finite difference technique for solving steady free-surface flows using orthogonal curvilinear coordinates', *AIChE J.*, **28**, 220–232 (1982).
13. T. J. Liu, T. A. Yu and S. H. Cheng, 'Finite difference solution of a Newtonian jet swell problem', *Int. j. numer. methods fluids*, **12**, 125–142 (1991).
14. H. Horsfall, 'A theoretical treatment of die swell in a Newtonian liquid', *Polymer*, **14**, 262–266 (1973).
15. G. A. Hill, C. A. Shook and M. N. Esmail, 'Finite difference simulaltion of die swell for a Newtonian fluid', *Canad. J. Chem. Eng.*, **59**, 100–108 (1981).
16. G. Ryskin and L. G. Leal, 'Numerical solution of free-boundary problems in fluid mechanics: Part I. The finite difference technique', *J. Fluid Mech.*, **148**, 1–17 (1984).
17. D. Dandy and L. G. Leal, 'A Newton's method scheme for solving free-surface flow problems', *Int. j. numer. methods fluids*, **9**, 1469–1486 (1989).
18. J. F. Thompson, F. C. Thomas and C. W. Mastin, 'Automatic numerical generation of body-fitted curvilinear coordinate system for field containing any number of arbitrary two-dimensional bodies', *J. Comput. Phys.*, **15**, 299–319 (1974).
19. J. F. Thompson, Z. U. A. Warsi and C. W. Mastin, 'Boundary-fitted coordinate systems for numerical solution of partial differential equations—a review', *J. Comput. Phys.*, **47**, 1–107 (1982).
20. T. A. Yu and T. J. Liu, 'An improved finite difference scheme for a Newtonian jet swell problem', *Int. j. numer. methods fluids*, **14**, 495–501 (1992).
21. G. Ryskin and L. G. Leal, 'Orthogonal Mapping', *J. Comput. Phys.*, **50**, 71–100 (1983).